Revised Version: 14th March 2008
Submission to CrystEngComm.

Correspondence to:
Simon Parsons
School of Chemistry
The University of Edinburgh
King's Buildings, West Mains Road
Edinburgh, Scotland, EH9 3JJ
Tel: 0131 650 4806
Fax: 0131 650 4743
Email: s.parsons@ed.ac.uk

A Study of the High-Pressure Polymorphs of L-Serine Using *Ab Initio* Structures and PIXEL Calculations

Peter A. Wood,[a] Duncan Francis,[b] William G. Marshall,[b] Stephen A. Moggach,[a] Simon Parsons,*[a] Elna Pidcock,[c] Andrew L. Rohl[d,e]

[a] School of Chemistry and Centre for Science at Extreme Conditions, The University of Edinburgh, King's Buildings, West Mains Road, Edinburgh, EH9 3JJ, UK. [b] ISIS Pulsed Neutron and Muon Facility, STFC Rutherford Appleton Laboratory, Harwell Science and Innovation Campus, Chilton, Didcot, OX11 0QX, UK. [c] Cambridge Crystallographic Data Centre, 12 Union Road, Cambridge, CB2 1EZ, UK. [d] iVEC, "The Hub of Advanced Computing in Western Australia", Perth, WA 6151, Australia. [e] Nanochemistry Research Institute, Department of Applied Chemistry, Curtin University of Technology, P.O. Box U1987, Perth, WA 6845, Australia.

ToC Synopsis

The crystal structures of L-serine phases I, II and III have been optimised at pressures from ambient pressure to 8.1 GPa using *ab initio* density functional theory. The phase-I to II transition is driven by a change in conformation of the serine molecules and a reduction in volume, while an intermolecular OH…carboxylate hydrogen bond strengthens during the II-to-III transition.

Abstract

Polymorphs of L-serine have been studied using *ab initio* density functional theory for pressures up to 8.1 GPa. The *SIESTA* code was used to perform geometry optimisations starting from the coordinates derived from high-pressure neutron powder diffraction. Between 0 and 8.1

GPa two phase transitions occur, the first of which takes place between 4.5 and 5.2 GPa and the second between 7.3 and 8.1 GPa. A change in molecular conformation occurs during the I-to-II transition, resulting in a stabilisation in intramolecular energy of 40 kJ mol^{-1}. There is good agreement between the theoretical and experimental coordinates, and the largest root-mean-square deviation between experimental and optimised structures is 0.121 Å. Analysis of the effect of pressure on the intermolecular interaction using the *PIXEL* method showed that none of the intermolecular interactions becomes significantly destabilising as the phase-I structure is compressed. It is proposed that the phase transition is driven by attainment of a more stable conformation and from the reduction in the molecular volume. The second phase transition occurs with only a small change in the hydrogen bonding pattern and no substantial difference in molecular conformation. The effect on the energies of attraction between molecules suggests that this transition is driven by the bifurcation of a short OH…O interaction.

Introduction

The experimental equipment and techniques involved in small molecule high-pressure crystallography are becoming accessible to more research groups. CCD detectors have improved the quality of data obtained and ease of structural determination.[1] This means that the number of structure determinations of molecular compounds at pressure has risen very quickly in recent years. The number of organic structures (with 3D coordinates) added per year to the Cambridge Structural Database (CSD) with the field 'pressure' included has risen from less than ten in all previous years to over 60 in both 2005 and 2006.

A number of pressure-induced phase transitions have been observed. These have been rationalised by analysis of the effects of pressure on intermolecular contact distances. Up to 10 GPa intermolecular interactions have so far been found to resist becoming significantly shorter than those of chemically similar contacts at ambient conditions, and phase transitions are observed once a lower distance limit has been reached. This idea has been used to 'explain' transitions due to short hydrogen bonds in L-serine-I[2] and close S…S contacts in L-cysteine-I.[3] In order to advance our understanding of the effects of pressure on crystal structures, and to learn more about why phase transitions occur, it is desirable to quantify the effect of compression on interaction *energies* rather than to use distance information alone.

L-serine undergoes two phase transitions at *ca.* 5 and 8 GPa.[4] The effect of pressure on the crystal structure of L-serine was studied using Raman spectroscopy single-crystal X-ray diffraction and neutron powder diffraction.[2, 4-8] The ambient pressure phase (L-serine-I) crystallises in space

group $P2_12_12_1$ and is made up of $C(5)$ chains along the *c*-axis formed by N1H5…O2 hydrogen bonds. Pairs of these chains are linked into ribbons by N1H6…O1 hydrogen bonds between molecules related by a 2_1 symmetry element, so forming repeated $R_3^3(11)$ ring motifs.[*9] The ribbons interact on both sides with adjacent ribbons *via* the hydroxyl side-chains to form an infinite O3H7…O3 hydrogen-bonded chain, thus forming layers in the *bc* plane (Figure 1a) which are referred to as the *A* layers by Moggach *et al.*[2] These layers are then linked together by N1H4…O2 hydrogen bonds in the *a*-direction thus forming another set of $C(5)$ chains and, when taken with the N1H5…O2 chains, they form another set of layers in the *ac* plane referred to as the *B* layers (Figure 2a).

The phase transition from phase I to phase II is isosymmetric and occurs with a 5% decrease in unit cell volume. In phase II the ribbons and $R_3^3(11)$ rings of phase I remain essentially unchanged except for some compression along the *c*-axis; in addition the hydroxyl groups rotate to form O3H7…O2 hydrogen bonds with the carboxyl group of a neighbouring chain (Figure 1b). This transition is therefore accompanied by a change in the conformation of the L-serine molecule (Figure 3). The layers are again linked together by N1H4…O2 hydrogen bonds (Figure 2b).

The second phase transition, from phase II to phase III, is also isosymmetric but does not involve a significant decrease in unit cell volume. The hydrogen bonding motifs remain largely the same during this phase transition except there is a shift of the *B* layers (Figure 2c) in the structure with respect to each other, causing the O3H7 hydrogen bond donor to form a bifurcated interaction, with O2 and O1 of separate molecules as acceptors.

Plane-wave density functional theory (DFT) provides quantification of overall interaction energies in the solid state.[10, 11] A second procedure, the *PIXEL* method,[12-16] allows calculation of lattice and intermolecular energies, and has been used, for example, in a study of the pressure-induced phase transition in the structure of salicylaldoxime-I.[17] In this paper we use a combination of DFT and *PIXEL* calculations to study the phase behaviour of L-serine at pressure up to 8.1 GPa with the aim of investigating the causes of the phase transitions.

Experimental

Neutron Crystal Structures

[*] Here $C(5)$ and $R^3_3(11)$ are graph set descriptors of hydrogen bonding motifs. $C(5)$ refers to a chain motif where the repeat unit in the chain is five atoms in length; $R^3_3(11)$ refers to an 11-membered ring motif containing three H-bond donors and three H-bond acceptors.

Ambient-temperature, high-pressure neutron powder diffraction data were collected on a sample of L-serine-d_7 (CDN Isotopes) by the time-of-flight technique at the PEARL high-pressure facility (HiPr) at ISIS.[18] The sample was contained in a TiZr capsule with a volume of 55 mm^3. Data sets between ambient pressure and 4.3 GPa were collected in the range $0.6 < d < 4.3$ Å using a V3b-type Paris-Edinburgh press using a 1:1 mixture of deuterated pentane and isopropanol as a hydrostatic medium; higher pressures were obtained using a second cell loading with a pressure medium consisting of a 4:1 mixture of deuterated methanol and ethanol. A small pellet of lead was included in the sample capsule to act as a pressure marker. Full details of the experiment have been published in an earlier paper.[4] The coordinates for the structures at 4.5, 5.2, 7.3 and 8.1 GPa have already been published in the CSD [refcodes LSERIN22 to LSERIN25], but full refinements of the structure of L-serine at all pressures for which data were collected between 0 and 8.1 GPa are reported here for the first time.

Crystal structure refinements

All crystal structure refinements were carried out using *TOPAS-Academic* version 4.1.[19]

The crystal structures of L-serine-I between 0.1 and 4.5 GPa were initially refined individually starting from the coordinates of a previous study at ambient conditions.[20] Using the Z-matrix formalism for rigid-body modelling available in *TOPAS*, the primary bond distances and angles were fixed at ambient pressure values, but the torsional angles, position and orientation of the molecules were allowed to refine. A common isotropic displacement parameter was refined for the C, N and O atoms; the H-atom displacement parameters were made equal to 1.2 (for CH and CH_2) or 1.5 (for OH and NH_3^+) times this value.

Though the intermolecular distances followed the expected downward trend, the variation was not smooth. Therefore, following a recent paper,[21] we tested a second modelling procedure where for a given phase all the neutron data sets were refined together, but with the displacement, position, orientation and torsion parameters all constrained to be a constant, linear or quadratic function of pressure. For example the displacement parameter could be modelled as either constant over all data sets, $B_{iso}(P) = a_0 + a_1P$ or $B_{iso}(P) = a_0 + a_1P + a_2P^2$ where P = pressure in GPa and the coefficients a_0, a_1 and a_2 were allowed to refine. Also included in the relevant refinements were a complete ambient pressure X-ray data set, the high pressure X-ray data sets reported by Moggach and coworkers[2] and a set of published single crystal X-ray structure factors obtained by Boldyreva for phase-III.[7] In short, all available high-pressure X-ray single crystal and neutron powder data sets were refined together for phases I, II and III.

It was found that, for phase-I, the position, orientation and the D7-O3-C3-C2 torsion could

be modelled as varying linearly with pressure; incorporation of a quadratic term did not improve the quality-of-fit, neither did allowing other torsional parameters to vary. No pressure dependence in the positional, orientation and torsional parameters was found to be necessary in the refinements for phases II and III.

Neither constraints nor restraints were applied to intermolecular distances. The primary bond distances and angles of the serine molecule were also refined freely for each phase – that is, the refinement models assumed that *within a particular phase* the bond distances and angles were invariant with pressure. A parameter representing the difference between X-ray and neutron distances to hydrogen was also refined. For the neutron data sets the pressure was calculated from the refined lead cell lattice parameter using a Birch-Murnaghan equation of state[22] with V_o = 30.3128 Å^3, B_o = 41.92 GPa, B' = 5.72. These parameters were derived by Fortes[23] as averages of the values determined in three earlier studies.[24-26] For the X-ray data sets the pressure was derived from ruby fluorescence measurements.[27]

The neutron structures were used for comparison with the *ab initio* theoretical structures discussed herein, and crystal and refinement data and inter- and intra-molecular distances are presented for the neutron refinements in Tables 1-3.

DFT Calculations

First principles electronic structure calculations were performed with the localised basis set pseudopotential method as employed in the code *SIESTA*.[28, 29] The starting point for each optimisation was the structure derived from neutron diffraction at a particular pressure. The unit cell dimensions were held fixed, while all other parameters were free to relax with no symmetry restrictions. The generalised gradient Perdew-Burke-Ernzerhof exchange correlation functionals were employed in the calculations.[30] Core electrons were represented by normconserving pseudopotentials of the form proposed by Troullier and Martins.[31] Valence electrons were described using double-ζ basis sets augmented with polarisation functions; full details are given in ref [32]. The basis sets in *SIESTA* are numerical ones, consisting of the exact solutions of the pseudopotential for the atomic state, except that a radial confinement is included to localise the orbital corresponding to an energy shift of 0.0001 Rydberg. A real space mesh equivalent to a plane wave cut-off of 250 Rydberg was used for the evaluation of the Hartree and exchange-correlation energies. The input files were prepared using the program *GDIS*.[33]

PIXEL Calculations

The final theoretical structures obtained were used to calculate the molecular electron density at each pressure using the program *GAUSSIAN98*[34] with the MP2/6-31G** basis set. The electron density model of the molecule was then analysed using the program package *OPiX*[35] which allows the calculation of dimer and lattice energies. Lattice energy calculations employed a cluster of molecules with maximum distance from the central molecule of 40 Å and a top radius for search of 50 Å. Calculations were also carried out for pairs of molecules identified in the lattice calculation as being energetically the most significant (*i.e.* with a magnitude > 2.5 kJ mol^{-1}). The output from these calculations yields a total energy and a breakdown into its Coulombic, polarisation, dispersion and repulsion components.[12-16]

Other Programs Used

Theoretical and experimental crystal structures were visualised using the programs *Mercury*[36] and *DIAMOND*.[37] Analyses were carried out using *PLATON*,[38] as incorporated in the *WinGX* suite.[39] Searches of the CSD[40, 41] utilised the program *ConQuest* and version 5.28 of the database with updates up to January 2007. Scatter-plots of intermolecular interaction geometries from the CSD were generated using the *IsoStar* library.[42]

The atom labelling scheme used (Scheme 1) is the same throughout the ambient-pressure and high-pressure datasets. This scheme also matches that used for L-serine in the previous two high-pressure studies.[2, 4]

Results

Comparison of the Experimental and Theoretical Intramolecular Geometries

Experimental crystal structure parameters were re-optimised using DFT calculations. The experimental primary bond distances and angles in L-serine I, II and III are compared to the average values for each phase of the theoretical structures in Table 3. Comparison of experimental and theoretical intramolecular geometries (*CRYSTALS*)[43 44] found that the root mean square deviation (RMSD) of bond lengths in the structures was never greater than 0.08 Å, and that in the positions was never larger than 0.15 Å. The largest variation with pressure in bond length in the theoretical data is 0.015 Å (for C1-O1 between phases I and II); this is within the precision of the experimentally determined structures at high pressure, and validates the commonly used procedure of restraining high-pressure structure refinements with bond distances derived at ambient pressure. With the exception of ∠C1C2N1, the trends in the theoretical and experimental bond angles (Table

3) are consistent. The C2-C3-O3 bond angle, for example, changes from approximately 112° to 106° between phases I and II in both sets of structures.

Comparison of the Experimental and Theoretical Intermolecular Geometries

A technique for comparing structures, which is used by the Crystal Structure Prediction (CSP) community, is to compare the relative coordinates of a cluster of 15 molecules in each structure. This comparison can be performed using the programs *COMPACK*[45] and *Mercury CSD 2.0*.[36] A root-mean-squared deviation (RMSD) is calculated over this cluster of 15 molecules for each comparison and a structural overlay is automatically carried out. For the purposes of this study the hydrogens were ignored for the comparison of structures. Comparison across the pressure series for L-serine yielded RMSD values of between 0.06 and 0.12 Å for the experimental *versus* theoretical structures. The largest deviation was seen for the structure of L-serine-III at 8.1 GPa which shows an RMSD of 0.121 Å between the neutron and *ab initio* structures. An example of the overlay between molecular clusters is shown in Figure 4 for L-serine-II at 5.2 GPa (RMSD of 0.105 Å) with the experimental structure in green and the theoretical structure in red. Typically, in the field of CSP, a matched (correctly predicted) structure will give an RMSD for this size of cluster of less than 1.0 Å compared to the experimental structure; values less than 0.2 Å are considered to be a very good match.[46]

Figure 5 shows the experimental and *ab initio* donor to acceptor distances for each of the shortest four hydrogen bonds as a function of pressure for the phase I structures of L-serine. Apart from the N1H5…O2 hydrogen bond, each of the theoretical compression curves matches well with that of the experimentally determined distances. A histogram illustrating the agreement between the observed (neutron) and calculated (*SIESTA*) H…O distances is shown in Figure 6. There is a tendency for the *SIESTA* distances to be too short, and the average deviation is 0.032 Å, though the full range is -0.250 to + 0.237 Å. A similar trend has been noted in DFT calculations of the O…O distance in the water dimer.[47]

The Response of the Theoretical Structure to Pressure

The data on the variation of the non-covalent interaction parameters in the theoretical and experimental structures between ambient pressure and 8.1 GPa are presented in Table 2. In the following we describe structural changes in terms of the *ab initio* results. The least compressible hydrogen bond during the compression of phase I is seen to be the shorter component of the bifurcated hydrogen bond N1H5…O2 (N1…O2 decreases by 1.7 % between ambient pressure and 4.5 GPa). The N1H6…O1 hydrogen bond is the next least compressible interaction, for which

N1…O1 decreases by 3.1 % to a distance of 2.689 Å at 4.5 GPa. The O3H7…O3 hydrogen bond compresses by 3.9 % from an O3…O3 distance of 2.891 at ambient pressure to 2.778 Å at 4.5 GPa. Finally, the last two hydrogen bonds, N1H5…O1 and N1H4…O2, which are relatively long at ambient pressure, decrease by 5.7 and 7.3 % respectively (N1…O1 decreases to 2.942 Å and N1…O2 is compressed to 2.699 Å at 4.5 GPa). The three main N…O distances all compress to approximately the same value (N1H5…O2 = 2.723 Å, N1H6…O1 = 2.689 Å and N1H4…O2 = 2.699 Å at 4.5 GPa).

The phase transition from L-serine-I to L-serine-II is accompanied by a *lengthening* of the N1H4…O2 hydrogen bond from 2.699 Å in phase I at 4.5 GPa to 2.834 Å in phase II at 5.2 GPa. The longer component of the bifurcated hydrogen bond, N1H5…O1, also becomes longer as the bifurcated character of this interaction decreases. The new OH…O interaction in the phase II structure (O3H7…O2)[4] is seen to be substantially shorter than the OH…O interaction in phase I (O3…O2 = 2.635 Å at 5.2 GPa).

In the transition from phase-II to phase-III each of the hydrogen bonds N1H5…O2/O1, N1H4…O2 and O3H7…O2 increases in length slightly during the shifting of the *B* layers with respect to each other. The hydrogen bond donor O3H7 forms a bifurcated hydrogen bond with O3H7…O2 being the major component (O3…O2 = 2.615 Å) and O3H7…O1 the minor component (O3…O1 = 2.940 Å). The only hydrogen bonding interaction distance that seen to decrease during this phase transition is N1H6…O1 (N1…O1 = 2.608 Å at 8.1 GPa).

Discussion

The Phase-I to II Transition

The pressure-induced phase transitions in the crystal structure of L-serine were rationalised in the previous two studies by analysis of the hydrogen bonding distances which developed on compression. As described above, each of the main NH…O interactions in the theoretical structures reaches a N…O distance of approximately 2.70 Å at 4.5 GPa, just before the phase transition to L-serine-II. A search of NH…O contact distances in the CSD for amino acid structures suggests that 2.70 Å approaches the minimum distance for this type of interaction, and we suggested that relief of strain in this contact 'drove' the transition from phase I to II.

A more general search of the Cambridge Structural Database (CSD) for any R_3NH^+ to $RCOO^-$ interactions in organic structures with R-factor <= 0.075 showed that there are a number of NH…O contacts shorter than the 2.70 Å limit, with the shortest N…O contact being 2.533 (2) Å for QIBSAV [1,4-diazabicyclo(2.2.2)octane bis(3,5-dinitrobenzoic acid) hydrate].[48] This implies that

that the conclusion reached in our previous study was based on too restrictive search criteria, and, notwithstanding the smaller steric effects between fragments located in the second search, it would appear that the hydrogen bonds in the phase-I structures are not yet at their ambient limits at 4.5 GPa. If this is the case then the phase transition is driven by some other factor. This aspect was investigated further using *PIXEL* calculations applied to the *ab initio*-optimised structures.

The *PIXEL* method is a technique that has been developed recently by Gavezzotti which allows substantial insight to be gained into the nature of intermolecular interactions through the calculation of crystal lattice and dimer energies. The technique is applied by determination of a molecular electron density map (using *GAUSSIAN*), condensation of the map into larger pixels and then calculation of energy terms between pairs of pixels in adjacent molecules. Recent studies using the program to analyse the compression of organic molecules,[16, 17, 49] have shown that the *PIXEL* technique is particularly useful for investigating the variation of intermolecular interactions with pressure.

The lattice energies of the L-serine theoretical structures and a breakdown into the component Coulombic, dispersion, polarisation and repulsion terms have been calculated and are shown in Table 4. In order to validate the energy calculations it is useful to compare the ambient pressure lattice enthalpy (-290.9 kJ mol^{-1}) with those determined using other techniques. The enthalpy of sublimation of L-serine has been experimentally determined[50] to be -173.6 kJ mol^{-1}, though proton transfer occurs between the ammonium and carboxylate groups during sublimation. If the proton transfer energy is taken into account[51] the lattice energy of zwitterionic serine is -279.9 kJ mol^{-1}, which is close to the value determined by the *PIXEL* method. The value of the lattice energy obtained from the *SIESTA* calculations using energies for the optimised structure of L-serine at ambient pressure and the fully-relaxed, non-zwitterionic, gas-phase molecule is -145.2 kJ mol^{-1}; this figure should be compared with -173.6 kJ mol^{-1}. The smaller theoretical value is expected because standard DFT functionals, such as those in *SIESTA*, underestimate the effect of dispersion forces.

The *PIXEL* method only calculates energies of interactions *between* molecules and any change in the internal energy of the molecule is not taken into account. There is, however, a change in the conformation of the L-serine molecule between phases I and II which is characterised by a rotations of the hydroxyl and amino groups and a twisting of the carbonyl group about the C1-C2 bond (Figure 3). *GAUSSIAN* calculations indicate that the energy associated with the conformational change is -40 kJ mol^{-1}, indicating that the molecular conformation in the ambient pressure structure is not optimal. A recent DFT study reached a similar conclusion for L-alanine, quoting a difference between the solid state and gas-phase conformations also of 40 kJ mol^{-1}.[52]

Table 4 includes a column showing an adjusted total energy (U_{adj}) which corresponds to the total lattice energy minus the difference in internal energy of the molecule as calculated by *GAUSSIAN*. Also displayed in the table are values for the enthalpy, $H = U_{adj} + PV$, where P = pressure and V = molar volume. Lattice enthalpy is plotted against pressure in Figure 7. Also shown in Figure 7 are the corresponding data derived from the *SIESTA* calculations; the agreement between the two methods is impressive. The effect of pressure on electron densities is only included implicitly in *PIXEL* calculations *via* the molecular geometry taken from a compressed crystal structure, and a referee of this paper questioned whether it is appropriate to neglect possible compression of the electron density. The agreement between the *PIXEL* and *SIESTA* energy changes, illustrated in Figure 7, shows that neglect of this effect (if it occurs) only introduces a small error.

The lattice enthalpy becomes more positive as pressure increases throughout each of the three phases due to the increasing repulsion and the pV terms. There is a discontinuity in the gradient of the graph near 5 GPa, where the phase transition from L-serine-I to L-serine-II takes place, the enthalpy of phase-II becoming more negative after the transition than the extrapolated values for phase-I. Inspection of the data in Table 4 shows that this can be ascribed to (i) the stabilisation of the internal energy of the serine molecules, and (ii) a diminution in the pV term as a structure with a smaller molecular volume is formed.

Intermolecular Interactions in L-Serine-I as a Function of Pressure

The *PIXEL* method also allows calculation of the intermolecular interaction energies between two molecules within the crystal structures. Six pairs of molecules in the L-serine-I theoretical crystal structure are found to have an attractive interaction energy greater than 2.5 kJ mol^{-1} at ambient pressure. These dimers, which are shown in Figure 8, are designated 1-6 in descending order of their interaction energy at ambient conditions; the variation in energy as a function of the centroid-centroid distance is also displayed in Figure 8. The data in Figure 8 were calculated with the *SIESTA*-optimised structures, but similar results are obtained when experimental data are used.

The dimer with the strongest interaction energy (1) at ambient conditions corresponds to the N1H4…O2 hydrogen bond in the L-serine-I structure. The next strongest interaction (2) is the bifurcated hydrogen bond N1H5…O1/O2. Interactions 3 and 4 relate to dimers which are not hydrogen bonded, 3 corresponds to a van der Waals contact and 4 corresponds to the interaction C3H3…O1. The final two interactions, 5 and 6, are also relatively weak and correspond to the hydrogen bonds N1H6…O1 and O3H7…O3 respectively.

The energy of interaction 5 (corresponding to the N1H6…O1 contact) seems to be small compared to the other charge-assisted NH…O hydrogen bonds: even though N1H5…O2 has similar H-bond geometric parameters to N1H6…O1 (Table 2), interaction 2 has an energy of -58.1 kJ mol^{-1} compared to -9.8 kJ mol^{-1} for interaction 5. Figure 9 shows an *IsoStar* contoured scatter-plot of intermolecular interactions between anionic $RCOO^-$ groups (fixed central fragment) and cationic RNH_3^+ groups (distribution around carboxylate) found within the CSD. The N-H donor group shows a distinct preference for H-bonding to either of the carboxylate lone pairs. The hydrogen bond corresponding to interaction 5 exhibits a contact between the lone pairs and out of the plane of the carboxylate group. These observations are consistent with a study of intermolecular contact energies in α-glycine,[53] which showed that there was also a weak hydrogen bond in that structure with a donor to acceptor geometry that would ordinarily suggest a strong interaction. This H-bond was also formed out of the plane of the carboxylate group. It is noticeable that the geometry of interaction 5 brings the carboxylate groups on neighbouring molecules relatively close to each other; the same is also true, though to a lesser extent, for the ammonium groups. The repulsion between like charges will lower the interaction energy for this intermolecular contact.

Although each of the six interactions has an increasing repulsion term with increasing pressure as the dimers are forced closer together, none of the interactions weaken considerably within this pressure regime. Three of the interactions (dimers 1, 2 and 4) are actually seen to strengthen as pressure is increased, whereas the remaining three interactions are only slightly weakened by the compression. Although these results are different to the behaviour of interactions seen in other pressure studies,[17] they are consistent with the conclusion (see above) that the I-to-II phase transition is not driven by relief of unfavourable contacts.

The Phase-II to III Transition

During the compression of phase II the N1H5…O2 hydrogen bond increases marginally, while the remaining interactions each decrease by 2% or less up to 7.3 GPa. With the exception of N1H6…O1, the H-bonds in L-serine-III at 8.1 GPa are actually longer than in phase-II prior to the phase transition. The main difference during the phase transition is the bifurcation of the O3H7…O2 interaction to form a hydrogen bond to a carbonyl acceptor (O1).

The conformation of the serine molecule does not change in moving from phase II to phase III, and the lattice enthalpy of phase III lies along the trend line established for phase II (Figure 7). *PIXEL* calculations (using the theoretical structural data) show that there are six important interactions in the phase II structure. These are labelled 1-6 in Figure 10 in descending order of interaction energy at 5.2 GPa; the variation of interaction energy with distance is also plotted in

Figure 10. Interaction 1 is again the N1H4…O2 hydrogen bond which was also the strongest interaction in phase I. The next strongest interactions, 2 & 3, are also the same as in the phase I structure, namely the N1H5…O1/O2 bifurcated hydrogen bond and a van der Waals contact, respectively. The fourth interaction is now the hydrogen bonded O3H7…O2 contact which replaced the O3H7…O3 contact during the phase transition. Finally interactions 5 & 6 correspond to another van der Waals contact and the hydrogen bonding interaction N1H6…O1 respectively.

The phase transition from phase-II to phase-III occurs with a marked increase in the attractive energy of interaction 5 which, in phase III, now corresponds to the newly formed minor component of the bifurcated hydrogen bond O3H7…O2/O1. It appears that the II-to-III transition is driven by a rearrangement into a more optimal intermolecular packing pattern.

Conclusions

We have described DFT geometry optimisations of the three phases of L-serine that exist between ambient pressure to 8.1 GPa and compared these structures to those determined using neutron powder diffraction. The theoretical structures are seen to compare very favourably with the experimental ones with only small differences in the primary geometry and molecular packing. These findings suggest that it may be possible to predict high pressure structures by performing a geometry relaxation on an ambient pressure structure using the *SIESTA* code with the addition of a fixed external pressure parameter.

PIXEL calculations show that there is a substantial energy gap between the intermolecular energies of phases I and II. Analysis of individual dimer energies also suggests that none of the intermolecular interactions becomes significantly destabilising as the transition pressure to phase-II is approached. The transition between phases I and II is driven partly by a change in molecular geometry to a conformer which is 40 kJ mol^{-1} more stable than that at ambient pressure. The phase transition also involves a substantial decrease in the unit cell volume which means a further stabilisation in enthalpy of phase II with respect to phase I.

Analysis of the intermolecular interaction energies during the compression of the phase II structure showed that the largest gain in energy during the second phase transition from L-serine-II to L-serine-III was in the formation of a bifurcated OH…O/O hydrogen bond.

Acknowledgements

We are very grateful to Prof. Angelo Gavezzotti (University of Milan) for his help and advice with our *PIXEL* calculations. We would also like the EPSRC and The Cambridge Crystallographic Data Centre for funding. Finally, this work was supported by iVEC through the use of advanced computing resources provided by the ARRC Facility in addition to computing time provided by the EaStCHEM Research Computing Facility.

References

1. A. Dawson, D. R. Allan, S. Parsons and M. Ruf, *J. Appl. Crystallogr.*, 2004, **37**, 410-416.

2. S. A. Moggach, D. R. Allan, C. A. Morrison, S. Parsons and L. Sawyer, *Acta Crystallogr., Sect. B*, 2005, **61**, 58-68.

3. S. A. Moggach, D. R. Allan, S. J. Clark, M. J. Gutmann, S. Parsons, C. R. Pulham and L. Sawyer, *Acta Crystallogr., Sect. B*, 2006, **62**, 296-309.

4. S. A. Moggach, W. G. Marshall and S. Parsons, *Acta Crystallogr., Sect. B*, 2006, **62**, 815-825.

5. E. V. Boldyreva, E. N. Kolesnik, H. Ahsbahs, J. A. Beukes and H.-P. Weber, *Z. Kristallogr.*, 2005, **220**, 58-57.

6. E. N. Kolesnik, S. V. Goryainov and E. V. Boldyreva, *Doklady Physical Chemistry*, 2005, **404**, 169-172.

7. T. N. Drebushchak, H. Sowa, Y. V. Seryotkin, E. V. Boldyreva and H. Ahsbahs, *Acta Crystallogr., Sect. E*, 2006, **62**, o4052-o4054.

8. E. V. Boldyreva, H. Sowa, Y. V. Seryotkin, T. N. Drebushchak, H. Ahsbahs, V. Chernyshev and V. Dmitriev, *Chem. Phys. Lett.*, 2006, **429**, 474-478.

9. J. Bernstein, R. E. Davis, L. Shimoni and N.-L. Chang, *Angewandte Chemie, International Edition*, 1995, **34**, 1555-1573.

10. C. A. Morrison and M. M. Siddick, *Chemistry - A European Journal*, 2003, **9**, 628-634.

11. R. Boese, A. J. Downs, T. M. Greene, A. W. Hall, C. A. Morrison and S. Parsons, *Organometallics*, 2003, **22**, 2450-2457.

12. J. D. Dunitz and A. Gavezzotti, *Angewandte Chemie, International Edition*, 2005, **44**, 1766-1787.

13. A. Gavezzotti, *Molecular Aggregation: Structure Analysis and Molecular Simulation of Crystals and Liquids*, Oxford University Press, Oxford, UK, 2007.

14. A. Gavezzotti, *CrystEngComm*, 2003, **5**, 429-438.

15. A. Gavezzotti, *Z. Kristallogr.*, 2005, **220**, 499-510.

16. A. Gavezzotti, *J.Phys.Chem. B*, 2002, **106**, 4145-4154.

17. P. A. Wood, R. S. Forgan, D. Henderson, S. Parsons, E. Pidcock, P. A. Tasker and J. E. Warren, *Acta Crystallogr., Sect. B*, 2006, **62**, 1099-1111.

18. Y. Le Godec, M. T. Dove, D. J. Francis, S. C. Kohn, W. G. Marshall, A. R. Pawley, G. D. Price, S. A. T. Redfern, N. Rhodes, N. L. Ross, P. F. Schofield, E. Schooneveld, G. Syfosse, M. G. Tucker and M. D. Welch, *Mineralogical Magazine*, 2001, **65**, 737-748.

19. A. A. Coelho, *TOPAS-Academic*, (2007) Bruker-AXS, Madison, Wisconsin, USA.

20. T. J. Kistenmacher, G. A. Rand and R. E. Marsh, *Acta Crystallogr., Sect. B*, 1974, **30**, 1610-1612.

21. G. W. Stinton and J. S. O. Evans, *J. Appl. Crystallogr.*, 2007, **40**, 87-95.

22. F. Birch, *Physical Review*, 1947, **71**, 809-824.

23. A. D. Fortes, PhD Thesis, University of London, 2004.

24. A. Z. Kuznetsov, V. Dmitriev, L. Dubrovinsky, V. Prakapenka and H. P. Weber, *Solid State Commun.*, 2002, **122**, 125-127.

25. R. A. Miller and D. E. Schuele, *J. Phys. Chem. Solids*, 1969, **30**, 589-600.

26. D. L. Waldorf and G. A. Alers, *J. Appl. Phys.*, 1962, **33**, 3266-3269.

27. G. J. Piermarini, S. Block, J. D. Barnett and R. A. Forman, *J. Appl. Phys.*, 1975, **46**, 2774-2780.

28. P. Ordejon, E. Artacho and J. M. Soler, *Physical Review B*, 1996, **53**, R10441-R10444.

29. J. M. Soler, E. Artacho, J. D. Gale, A. Garcia, J. Junquera, P. Ordejon and D. Sanchez-Portal, *J. Phys.: Condens. Matter*, 2002, **14**, 2745–2779.

30. J. P. Perdew, K. Burke and M. Ernzerhof, *Phys. Rev. Lett.*, 1996, **77**, 3865-3868.

31. N. Troullier and J. L. Martins, *Phys. Rev. B: Condens. Matter*, 1991, **43**, 1993-2006.

32. J. Junquera, O. Paz, D. Sanchez-Portal and E. Artacho, *Phys. Rev. B: Condens. Matter*, 2001, **64**, 235111.

33. S. Fleming and A. Rohl, *Z. Kristallogr.*, 2005, **220**, 580–584.

34. M. J. Frisch, G. W. Trucks, H. B. Schlegel, G. E. Scuseria, M. A. Robb, J. R. Cheeseman, V. G. Zakrzewski, J. A. J. Montgomery, R. E. Stratmann, J. C. Burant, S. Dapprich, J. M. Millam, A. D. Daniels, K. N. Kudin, M. C. Strain, O. Farkas, J. Tomasi, V. Barone, M. Cossi, R. Cammi, B. Mennucci, C. Pomelli, C. Adamo, S. Clifford, J. Ochterski, G. A. Petersson, P. Y. Ayala, Q. Cui, K. Morokuma, D. K. Malick, A. D. Rabuck, K. Raghavachari, J. B. Foresman, J. Cioslowski, J. V. Ortiz, B. B. Stefanov, G. Liu, A. Liashenko, P. Piskorz, I. Komaromi, R. Gomperts, R. L. Martin, D. J. Fox, T. Keith, M. A. Al-Laham, C. Y. Peng, A. Nanayakkara, C. Gonzalez, M. Challacombe,

P. M. W. Gill, B. G. Johnson, W. Chen, M. W. Wong, J. L. Andres, M. Head-Gordon, E. S. Replogle and J. A. Pople, *Gaussian 98 revision A.7*, (1998) Gaussian, Inc., Pittsburgh, PA, USA.

35. A. Gavezzotti, *OPiX: A computer program package for the calculation of intermolecular interactions and crystal energies.*, (2003), University of Milan, Italy.

36. C. F. Macrae, I. J. Bruno, J. A. Chisholm, P. R. Edgington, P. McCabe, E. Pidcock, L. Rodriguez-Monge, R. Taylor, J. van de Streek and P. A. Wood, *J. Appl. Crystallogr.*, 2008, submitted.

37. Crystal Impact, *DIAMOND version 3.0*, (2004) Crystal Impact GbR, Postfach 1251, 53002, Bonn, Germany.

38. A. L. Spek, *J. Appl. Crystallogr.*, 2003, **36**, 7-13.

39. L. J. Farrugia, *J. Appl. Crystallogr.*, 1999, **32**, 837-838.

40. F. H. Allen, *Acta Crystallogr., Sect. B*, 2002, **58**, 380-388.

41. F. H. Allen and W. D. S. Motherwell, *Acta Crystallogr., Sect. B*, 2002, **58**, 407-422.

42. I. J. Bruno, J. C. Cole, J. P. M. Lommerse, R. S. Rowland, R. Taylor and M. L. Verdonk, *Journal of Computer-Aided Materials Design*, 1997, **11**, 525-537.

43. P. W. Betteridge, J. R. Carruthers, R. I. Cooper, K. Prout and D. J. Watkin, *J. Appl. Crystallogr.*, 2003, **36**, 1487.

44. A. Collins, R. I. Cooper and D. J. Watkin, *J. Appl. Crystallogr.*, 2006, **39**, 842-849.

45. J. A. Chisholm and S. Motherwell, *J. Appl. Crystallogr.*, 2005, **38**, 228-231.

46. G. M. Day, W. D. S. Motherwell, H. L. Ammon, S. X. M. Boerrigter, R. G. Della Valle, E. Venuti, A. Dzyabchenko, J. D. Dunitz, B. Schweizer, B. P. Van Eijck, P. Erk, J. C. Facelli, V. E. Bazterra, M. B. Ferraro, D. W. M. Hofmann, F. J. J. Leusen, C. Liang, C. C. Pantelides, P. G. Karamertzanis, S. L. Price, T. C. Lewis, H. Nowell, A. Torrisi, H. A. Scheraga, Y. A. Arnautova, M. U. Schmidt and P. Verwer, *Acta Crystallogr., Sect. B*, 2005, **61**, 511-527.

47. W. Koch and M. C. Holthausen, in *A Chemist's Guide to Density Functional Theory*, Wiley-VCH, Weinheim, Germany., Editon edn., 2000, p. 219.

48. C. J. Burchell, C. Glidewell, A. J. Lough and G. Ferguson, *Acta Crystallogr., Sect. B*, 2001, **57**, 201-212.

49. P. A. Wood, D. A. Haynes, A. R. Lennie, W. D. S. Motherwell, S. Parsons, E. Pidcock and J. E. Warren, *Crystal Growth & Design*, 2008, in press.

50. C. G. de Kruif, J. Voogd and J. C. A. Offringa, *J. Chem. Thermodyn.*, 1979, **11**, 651-656.

51. T. N. Kyoung, H. C. Kwang, O. Y. Kwon, M. S. Jhon and H. A. Scheraga, *J. Phys. Chem.*, 1994, **98**, 10742-10749.

52. T. G. Cooper, W. Jones, W. D. S. Motherwell and G. M. Day, *CrystEngComm*, 2007, **9**, 595-602.

53. A. Volkov and P. Coppens, *J. Comput. Chem.*, 2004, **25**, 921-934.

Schemes

Scheme 1: Chemical structure diagram showing atomic numbering scheme.

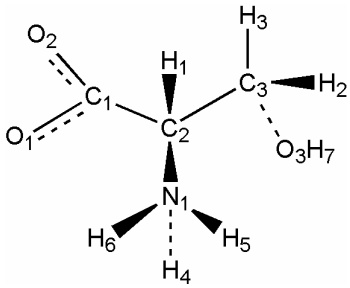

Table 1: Crystallographic data for neutron powder diffraction study of L-serine at increasing pressures; L-serine-I (ambient to 4.5 GPa), L-serine-II (5.2 to 7.3 GPa) and L-serine-III (8.1 GPa).

Phase	**Serine-I**	**Serine-I**	**Serine-I**	**Serine-I**	**Serine-I**
Pressure (GPa)	0.076(8)	0.940(8)	1.613(9)	2.625(9)	3.458(10)
Chemical formula			$C_3D_7NO_3$		
M_r			112.11		
Cell setting, space group	Orthorhombic, $P2_12_12_1$	Orthorhombic, $P2_12_12_1$	Orthorhombic, $P2_12_12_1$	Orthorhombic, $P2_12_12_1$	Orthorhombic, $P2_12_12_1$
Temperature (K)	298	298	298	298	298
a, b, c (Å)	8.5720 (7) 9.3012 (5) 5.6043 (5)	8.4877 (7) 9.0943 (5) 5.5754 (5)	8.4435 (7) 8.9641 (6) 5.5546 (5)	8.3918 (7) 8.8060 (5) 5.5219 (5)	8.3547 (7) 8.7062 (5) 5.4968 (5)
V (Å^3)	446.83 (6)	430.36 (6)	420.43 (6)	408.05 (6)	399.82 (6)
Z	4	4	4	4	4
D_x (Mg m^{-3})	1.666	1.730	1.771	1.825	1.862
R factors and goodness of fit	R_p = 3.222, R_{wp} = 2.845, R_{exp} = 1.821, S = 1.56	R_p = 3.290, R_{wp} = 2.974, R_{exp} = 1.855, S =1.60	R_p = 3.142, R_{wp} = 2.848, R_{exp} = 1.976, S =1.48	R_p = 3.085, R_{wp} = 2.848, R_{exp} = 1.917, S =1.48	R_p = 3.049, R_{wp} = 2.522, R_{exp} = 1.961, S =1.29
No. of parameters			273		
	Serine-I	**Serine-I**	**Serine-II**	**Serine-II**	**Serine-II**
Pressure (GPa)	4.270(8)	4.514(15)	5.199(16)	5.700(17)	6.28(2)
Chemical formula			$C_3D_7NO_3$		
M_r			112.11		
Cell setting, space group	Orthorhombic, $P2_12_12_1$	Orthorhombic, $P2_12_12_1$	Orthorhombic, $P2_12_12_1$	Orthorhombic, $P2_12_12_1$	Orthorhombic, $P2_12_12_1$
Temperature (K)	298	298	298	298	298
A, b, c (Å)	8.3216 (6) 8.6243 (4) 5.4739 (4)	8.3099 (5) 8.5951 (4) 5.4658 (4)	6.8700 (3) 9.6373 (6) 5.6066 (3)	6.8107 (4) 9.6227 (7) 5.5934 (3)	6.7627 (4) 9.6073 (7) 5.5825 (4)
V (Å^3)	392.85 (5)	390.39 (4)	371.21 (3)	366.58 (4)	362.70 (4)
Z	4	4	4	4	4
D_x (Mg m^{-3})	1.895	1.907	2.006	2.031	2.053
R factors and goodness of fit	R_p = 2.735, R_{wp} = 2.232, R_{exp} = 1.567, S = 1.42	R_p = 2.720, R_{wp} = 2.223, R_{exp} = 1.659, S = 1.34	R_p = 2.879, R_{wp} = 2.555, R_{exp} = 1.541, S = 1.66	R_p = 2.939, R_{wp} = 2.596, R_{exp} = 1.616, S = 1.61	R_p = 3.202, R_{wp} = 2.552, R_{exp} = 1.877, S = 1.36
No. of parameters	273			141	
	Serine-II	**Serine-III**			
Pressure (GPa)	7.243(19)	8.162(18)			
Chemical formula	$C_3D_7NO_3$				
M_r	112.11				
Cell setting, space group	Orthorhombic, $P2_12_12_1$	Orthorhombic, $P2_12_12_1$			
Temperature (K)	298	298			
a, b, c (Å)	6.6869 (3) 9.5802 (6) 5.5624 (3)	6.5487 (3) 9.5386 (5) 5.6078 (3)			
V (Å^3)	356.34 (3)	350.30 (3)			
Z	4	4			
D_x (Mg m^{-3})	2.089	2.125			
R factors and goodness of fit	R_p = 2.961, R_{wp} = 2.503, R_{exp} = 1.602, S = 1.56	R_p = 3.017, R_{wp} = 2.407, R_{exp} = 1.834, S = 1.31			
No. of parameters	141	58			

Table 2: Non-covalent interaction parameters in the L-serine theoretical and experimental crystal structures. The theoretical values are shown first and the experimental values given in italics. Distances are in Å and angles in degrees. The Δ column refers to the D...A distance at the highest pressure obtained for phase I (4.5 GPa) subtracted from the same distance at the lowest pressure obtained (ambient).

Pressure/GPa	0.0	0.1	0.9	1.7	2.7	3.5	4.3	4.5	Δ (I)
N1H5..O2[i]									
H5..O2	1.73	1.74	1.72	1.71	1.72	1.71	1.69	1.71	
	1.990(10)	*1.930(6)*	*1.909(6)*	*1.894(6)*	*1.871(6)*	*1.853(6)*	*1.837(6)*	*1.832(6)*	
N1..O2	2.771	2.781	2.753	2.740	2.747	2.729	2.716	2.723	0.048
	2.887(5)	*2.875(5)*	*2.851(5)*	*2.834(5)*	*2.807(5)*	*2.786(5)*	*2.768(5)*	*2.761(5)*	*0.126*
<N1H5O2	165	165	164	163	162	161	161	160	
	154(3)	*153(1)*	*152(1)*	*152(1)*	*151(1)*	*151(1)*	*150(1)*	*150(1)*	
N1H5..O1[i]									
H5..O1	2.34	2.30	2.31	2.28	2.21	2.20	2.19	2.16	
	2.304(11)	*2.246(6)*	*2.220(6)*	*2.201(6)*	*2.171(6)*	*2.148(6)*	*2.127(6)*	*2.120(6)*	
N1..O1	3.119	3.064	3.080	3.056	2.985	2.973	2.954	2.942	0.177
	3.124(5)	*3.109(5)*	*3.081(5)*	*3.061(5)*	*3.029(5)*	*3.004(5)*	*2.982(5)*	*2.974(5)*	*0.150*
<N1H5O1	128	128	128	128	128	128	128	129	
	142(2)	*141(1)*	*141(1)*	*141(1)*	*141(1)*	*140(1)*	*140(1)*	*140(1)*	
N1H4..O2[ii]									
H4..O2	1.88	1.86	1.80	1.78	1.74	1.71	1.70	1.68	
	1.967(8)	*1.902(5)*	*1.856(5)*	*1.831(5)*	*1.803(5)*	*1.783(6)*	*1.767(6)*	*1.761(6)*	
N1..O2	2.911	2.886	2.827	2.804	2.763	2.732	2.713	2.699	0.212
	2.879(4)	*2.866(4)*	*2.813(4)*	*2.784(4)*	*2.748(4)*	*2.723(5)*	*2.700(5)*	*2.693(5)*	*0.186*
<N1H4O2	163	163	163	161	161	160	159	160	
	157(3)	*156(2)*	*155(1)*	*154(1)*	*153(1)*	*152(1)*	*150(1)*	*150(1)*	
N1H6..O1[iii]									
H6..O1	1.75	1.76	1.73	1.72	1.69	1.69	1.67	1.66	
	1.938(9)	*1.865(5)*	*1.808(5)*	*1.776(5)*	*1.743(5)*	*1.727(5)*	*1.718(6)*	*1.713(6)*	
N1..O1	2.775	2.788	2.753	2.741	2.720	2.712	2.695	2.689	0.086
	2.858(4)	*2.837(4)*	*2.781(4)*	*2.750(4)*	*2.718(4)*	*2.703(4)*	*2.695(5)*	*2.690(5)*	*0.168*
<N1H6O1	162	163	162	162	163	163	163	163	
	159(4)	*158(2)*	*158(2)*	*158(2)*	*159(2)*	*159(2)*	*159(2)*	*159(2)*	
O3H7..O3[iv]									
H7..O3	1.95	1.95	1.92	1.90	1.89	1.87	1.86	1.84	
	2.103(14)	*2.038(11)*	*2.002(13)*	*1.981(15)*	*1.96(2)*	*1.94(2)*	*1.93(4)*	*1.93(4)*	
O3..O3	2.891	2.884	2.852	2.837	2.817	2.795	2.783	2.778	0.113
	2.923(3)	*2.906(3)*	*2.863(2)*	*2.839(2)*	*2.812(2)*	*2.796(2)*	*2.786(2)*	*2.782(2)*	*0.141*
<O3H7O3	158	157	158	157	156	155	154	156	
	155(4)	*154(2)*	*152(3)*	*152(3)*	*151(4)*	*151(5)*	*150(7)*	*150(7)*	

Pressure/GPa	5.2	5.8	6.3	7.3	8.1
N1H5..O2[i]					
H5..O2	1.65	1.65	1.66	1.67	1.67
	1.887(13)	*1.877(13)*	*1.869(13)*	*1.855(13)*	*1.82(3)*
N1..O2	2.686	2.686	2.694	2.692	2.708
	2.836(12)	*2.825(12)*	*2.816(12)*	*2.799(12)*	*2.81(2)*
<N1H5O2	164	163	163	162	164
	152(3)	*152(3)*	*152(3)*	*151(3)*	*160(9)*
N1H5..O1[i]					
H5..O1	2.38	2.37	2.34	2.31	2.37
	2.221(13)	*2.209(13)*	*2.199(13)*	*2.180(13)*	*2.32(3)*
N1..O1	3.185	3.171	3.139	3.120	3.165
	3.099(12)	*3.086(12)*	*3.075(12)*	*3.056(12)*	*3.14(3)*
<N1H5O1	131	131	131	132	131
	142(2)	*142(2)*	*142(2)*	*142(2)*	*135(4)*
N1H4..O2[ii]					
H4..O2	1.81	1.80	1.80	1.79	1.83
	1.861(11)	*1.835(11)*	*1.814(11)*	*1.782(11)*	*1.84(2)*
N1..O2	2.834	2.819	2.822	2.806	2.836
	2.832(9)	*2.805(9)*	*2.783(9)*	*2.749(9)*	*2.828(18)*
<N1H4O2	164	164	164	162	161
	157(3)	*156(3)*	*156(3)*	*155(3)*	*158(6)*
N1H6..O1[iii]					
H6..O1	1.66	1.65	1.63	1.63	1.57
	1.745(11)	*1.734(11)*	*1.723(11)*	*1.705(11)*	*1.675(19)*
N1..O1	2.654	2.643	2.632	2.622	2.608
	2.644(10)	*2.635(10)*	*2.627(10)*	*2.612(10)*	*2.642(17)*
<N1H6O1	157	157	158	157	165
	144(2)	*144(2)*	*144(2)*	*145(2)*	*154(5)*
O3H7..O2[iv]					
H7..O2	1.64	1.63	1.62	1.60	1.68
	1.639(16)	*1.629(16)*	*1.619(16)*	*1.602(16)*	*1.84(3)*
O3..O2	2.635	2.625	2.614	2.599	2.615
	2.630(13)	*2.629(13)*	*2.608(13)*	*2.590(13)*	*2.66(3)*
<O3H7O2	173	173	173	172	155
	169(10)	*168(10)*	*168(10)*	*167(9)*	*136(5)*
O3H7..O1[v]					
H7..O1	-	-	-	-	2.38
	-	-	-	-	*2.13(3)*
O3..O1	-	-	-	-	2.940
					2.89(3)
<O3H7O1					114
					131(4)

Symmetry Operators:

i	$x,y,1+z$
ii	$-1/2+x,3/2-y,1-z$
iii	$3/2-x, 2-y,1/2+z$
iv	$3/2-x, 1-y,1/2+z$
v	$1-x, -1/2+y,3/2-z$

Table 3: Average non-hydrogen bond lengths and angles in the experimental and theoretical structures of L-serine. For the neutron structures the non-hydrogen primary bond lengths and angles were assumed to be constant for a given phase during refinement. The theoretical values shown are the averages of the parameters for the structures within each phase. Bond lengths are in Å and bond angles are in degrees.

	Neutron Phase I	**Neutron Phase II**	**Neutron Phase III**	**SIESTA Phase I**	**SIESTA Phase II**	**SIESTA Phase III**
C1-C2	1.536 (2)	1.492 (5)	1.504 (10)	1.537	1.534	1.531
C2-C3	1.528 (2)	1.539 (5)	1.511 (8)	1.536	1.529	1.526
C1-O1	1.2303 (19)	1.222 (6)	1.266 (8)	1.268	1.253	1.257
C1-O2	1.2583 (19)	1.279 (5)	1.266 (8)	1.282	1.293	1.286
C3-O3	1.4225 (18)	1.437 (3)	1.402 (11)	1.432	1.422	1.428
C2-N1	1.4899 (18)	1.520 (3)	1.483 (7)	1.479	1.476	1.474
∠C1C2C3	109.94 (10)	111.1 (2)	110.7 (3)	111.7	113.0	113.6
∠C1C2N1	109.33 (10)	109.2 (2)	110.7 (4)	111.8	107.9	108.2
∠C2C1O1	119.21 (13)	117.2 (4)	114.0 (8)	118.5	117.7	117.5
∠C2C1O2	114.60 (13)	119.5 (4)	121.4 (6)	116.3	118.1	118.4
∠C2C3O3	111.97 (13)	105.6 (3)	105.9 (6)	112.2	106.0	106.7
∠C3C2N1	109.31(7)	108.78(15)	108.2(3)	110.3	108.3	108.1

Table 4: The components of lattice energy and the total energy at each pressure (GPa) for L-serine theoretical structures (energies in kJ mol^{-1}) along with the adjusted total energy (U_{adj}) and the enthalpy (H).

Pressure/ GPa	Coulombic	Polarisation	Dispersion	Repulsion	Total Energy	U_{adj}*	$H^{\dagger}$
0.0	-319.8	-121.6	-85.1	235.6	-290.9	-290.9	-290.9
0.1	-320.9	-122.6	-86.9	239.6	-290.7	-286.7	-280.0
0.9	-341.3	-134.3	-94.8	279.6	-290.8	-289.6	-231.3
1.7	-350.3	-140.5	-99.9	302.5	-288.2	-287.9	-180.3
2.7	-368.1	-151.1	-107.3	335.8	-290.8	-286.5	-120.6
3.5	-376.4	-157.1	-112.3	364.9	-280.9	-276.8	-66.2
4.3	-389.0	-165.9	-117.1	393.8	-278.1	-273.8	-19.7
4.5	-395.2	-170.9	-118.7	403.9	-280.9	-277.1	-12.7
5.2	-388.7	-162.1	-129.7	452.2	-228.4	-268.1	22.5
5.8	-396.4	-167.4	-133.5	473.3	-223.9	-262.7	57.3
6.3	-404.2	-171.0	-136.8	490.8	-221.2	-259.8	84.0
7.3	-413.5	-178.4	-141.9	517.3	-216.6	-255.2	136.4
8.1	-428.7	-180.0	-149.4	547.6	-210.5	-246.8	180.5

***** Adjusted Energy (U_{adj}) = Total Energy – Energy difference due to conformation change relative to 0.0 GPa structure based on *GAUSSIAN98* calculation.

† Enthalpy (H) = $U_{adj} + PV$, where P = pressure (in Pascals) and V = molar volume (in $m^3\ mol^{-1}$).

Figure 1: The effect of pressure on the theoretical crystal structure of L-serine as viewed along the *a*-axis: (*a*) L-serine-I at ambient pressure; (*b*) L-serine-II at 5.2 GPa; (*c*) L-serine-III at 8.1 GPa; H7 bifurcates between the interaction shown and with O1 in the next layer up. This layer is referred to as the *A* layer in the text. The colour scheme is red: oxygen, blue: nitrogen, light-grey: carbon and hydrogen: dark-grey.

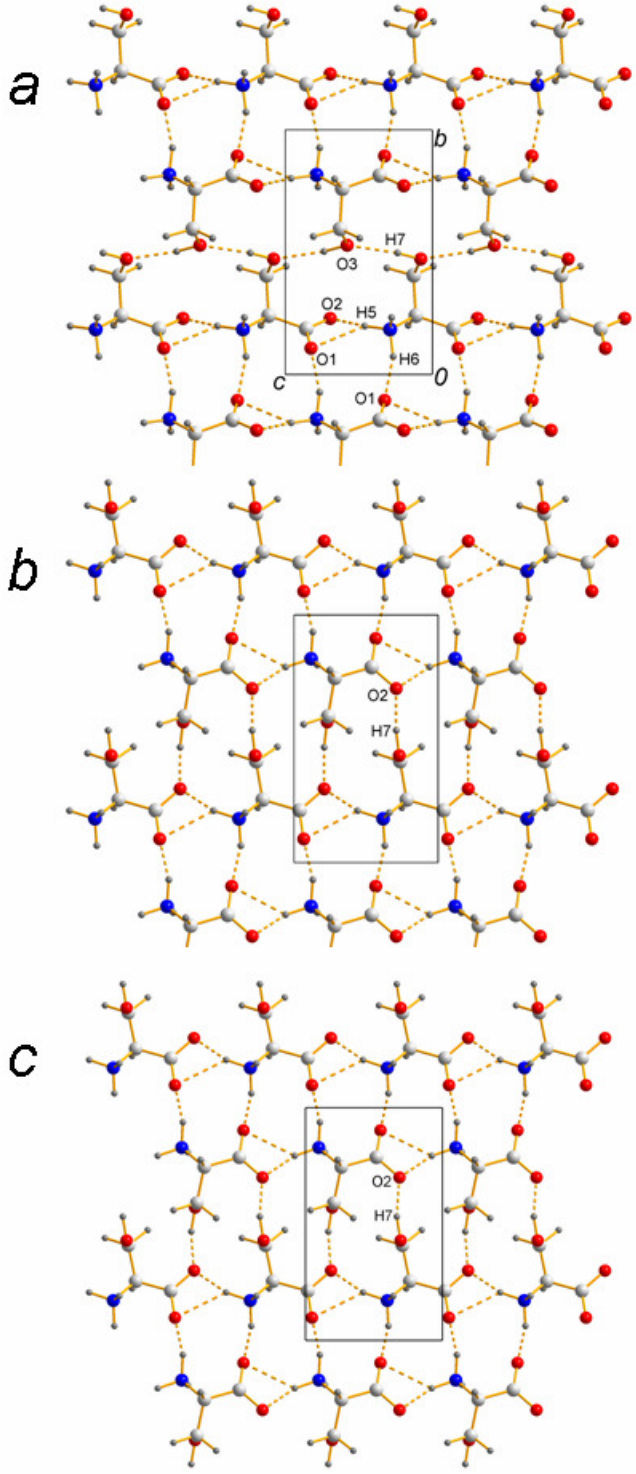

Figure 2: The effect of pressure on the theoretical crystal structure of L-serine as viewed along the *b*-axis: (*a*) L-serine-I at ambient pressure; (*b*) L-serine-II at 5.2 GPa; (*c*) L-serine-III at 8.1 GPa. This layer is referred to as the *B* layer in the text. The colour scheme is the same as in Fig. 1.

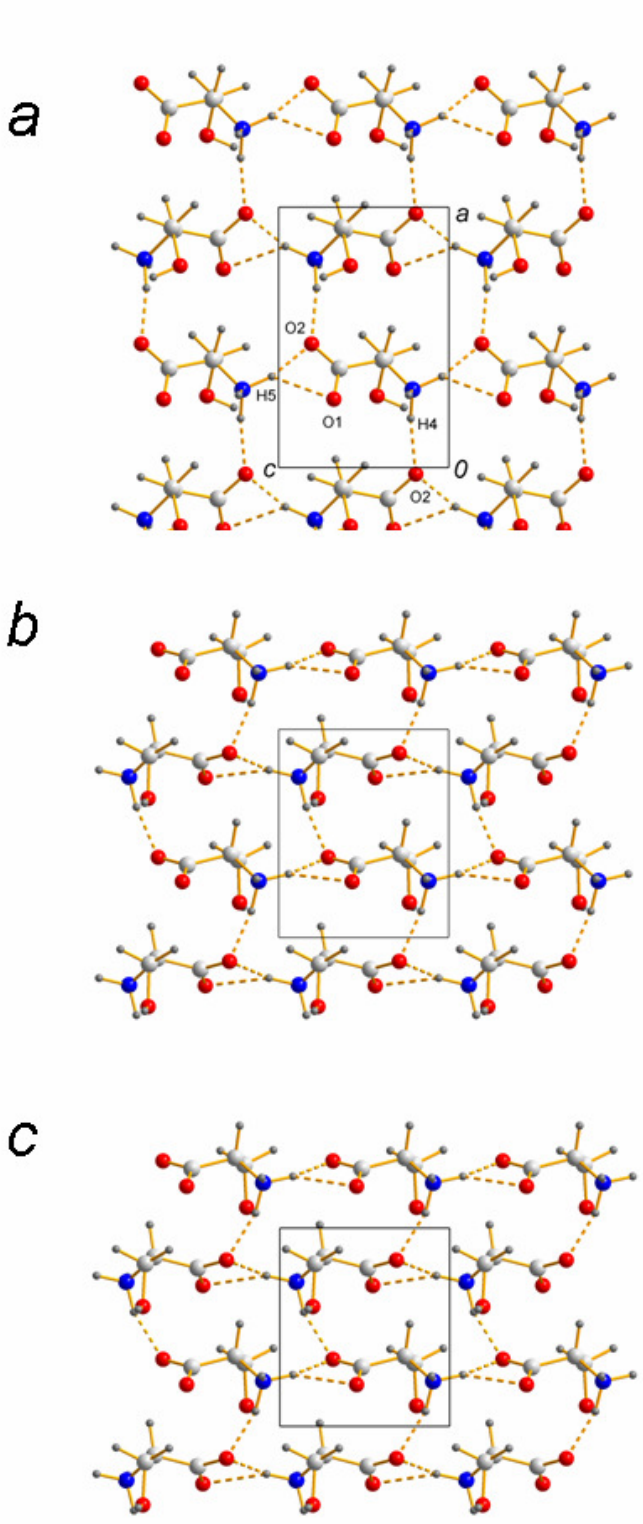

Figure 3: Structure overlay showing the change in conformation of the L-serine molecule between phase I at 4.5 GPa (coloured by element) and phase-II at 5.2 GPa (green). The overlay shows the rotation of the hydroxyl group, a twisting of the carboxyl group and a slight rotation of the amino group. The colour scheme for the phase-I structure is red: oxygen, blue: nitrogen, light-grey: carbon and white: hydrogen.

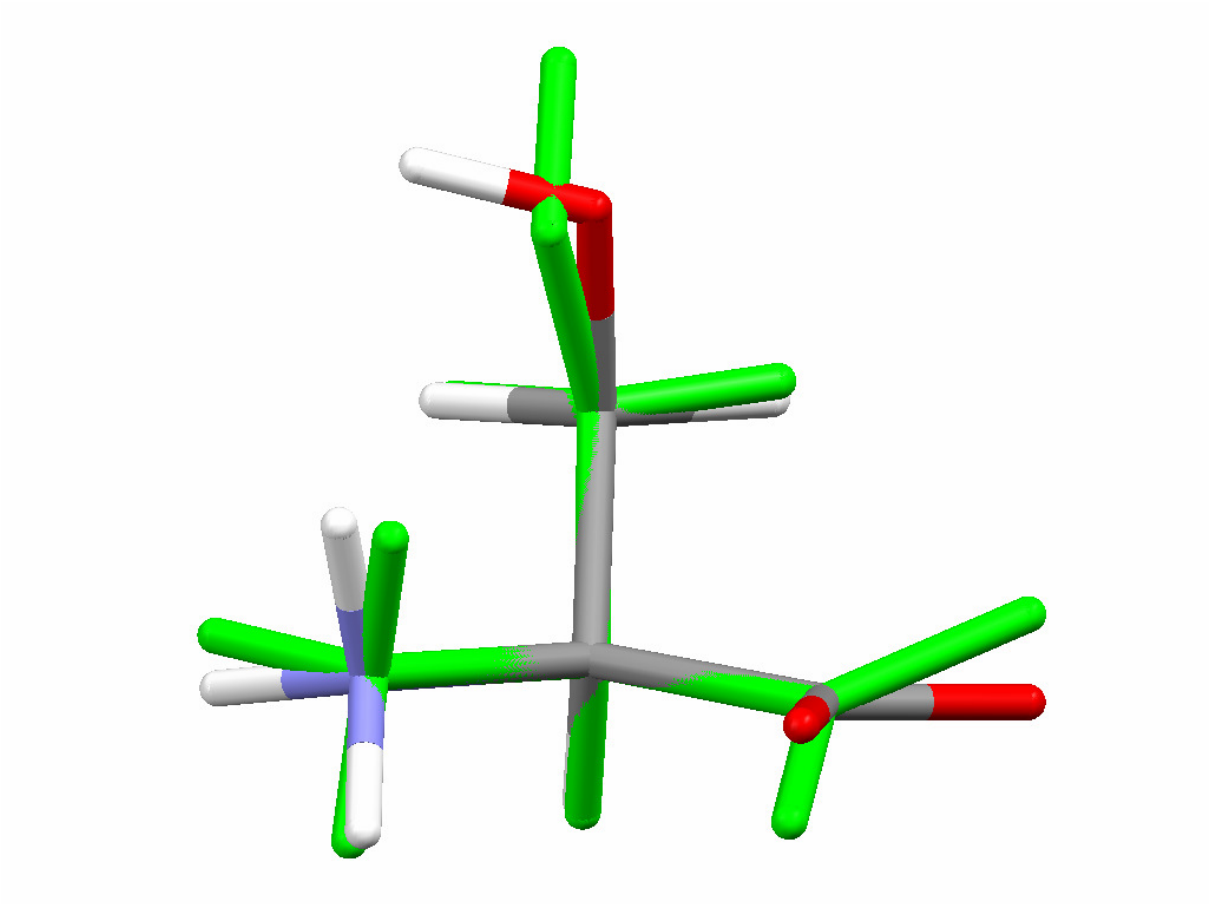

Figure 4: Structural overlay of a 15 molecule cluster in the L-serine-II experimental structure at 5.2 GPa (green) with the equivalent theoretical structure (red). Hydrogen atoms have been removed for clarity. The RMSD for this cluster comparison is 0.105 Å over the whole cluster at this pressure.

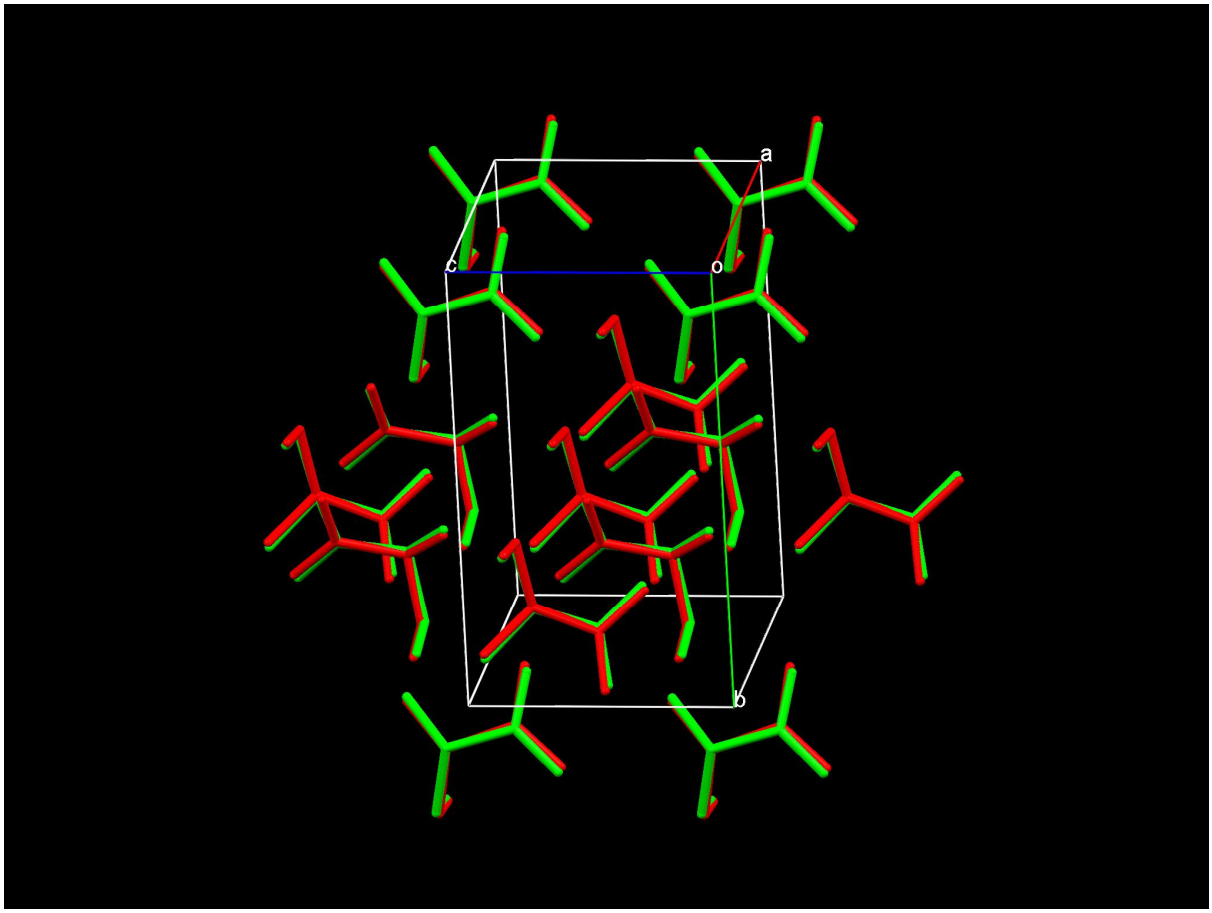

Figure 5: Graphs of hydrogen bond donor to acceptor distances (in Å) as a function of pressure (in GPa) for the interactions N1(H5)…O2 (a), N1(H4)…O2 (b), N1(H6)…O1 (c) and O3(H7)…O3 (d) in L-serine-I. The data are shown in each graph for the neutron powder structures (green) and the *SIESTA* theoretical structures (red). Error bars have been displayed for the interactions in the experimental structures at the 1 σ level. Each plot is shown on the same scale using distances from 2.6 to 3.0 Å and pressures from 0.0 to 5.0 GPa.

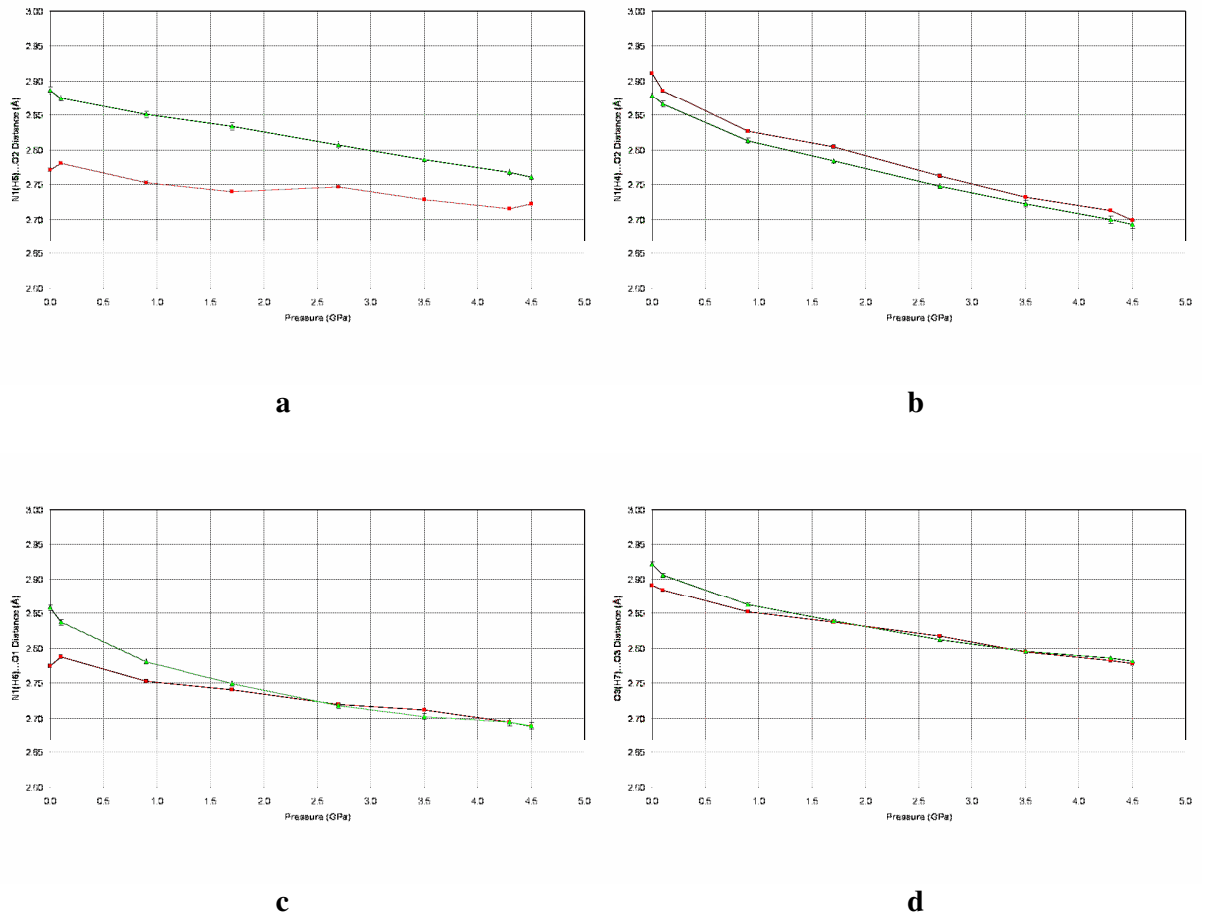

a **b**

c **d**

Figure 6: Histogram showing the deviation between observed (neutron) and calculated (*SIESTA*) O…H distances (in Å) in serine I, II and III at pressures between ambient and 8.1 GPa.

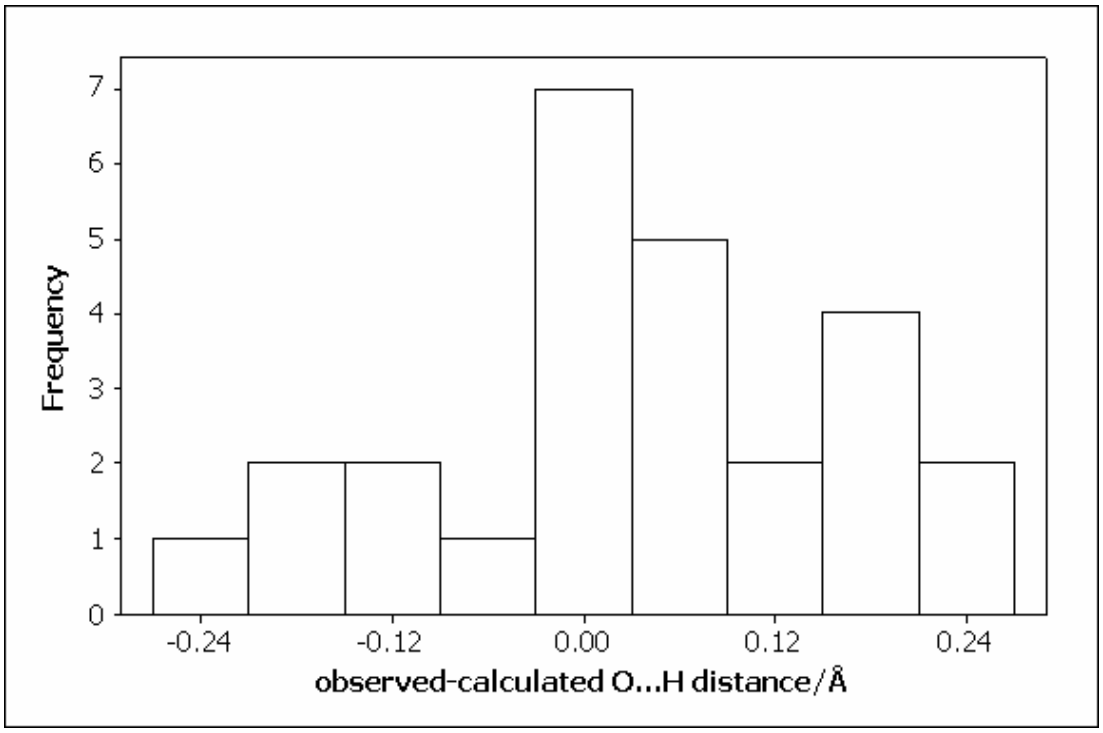

Figure 7: Graph of theoretical structure lattice enthalpy (in kJ mol^{-1}) of the three phases of L-serine as a function of pressure (in GPa) calculated by the *PIXEL* and DFT (*SIESTA*) methods. DFT calculate total energies involving all electronic and nuclear interactions and are orders of magnitude different to *PIXEL* energies. For the purposes of this comparison the points plotted for the *SIESTA* calculations are $H_{Scaled\_SIESTA} = H_{SIETSA} + \overline{H_{PIXEL} - H_{SIESTA}}$, where $\overline{H_{PIXEL} - H_{SIESTA}}$ is the mean difference between the *PIXEL* and *SIESTA* enthalpies.

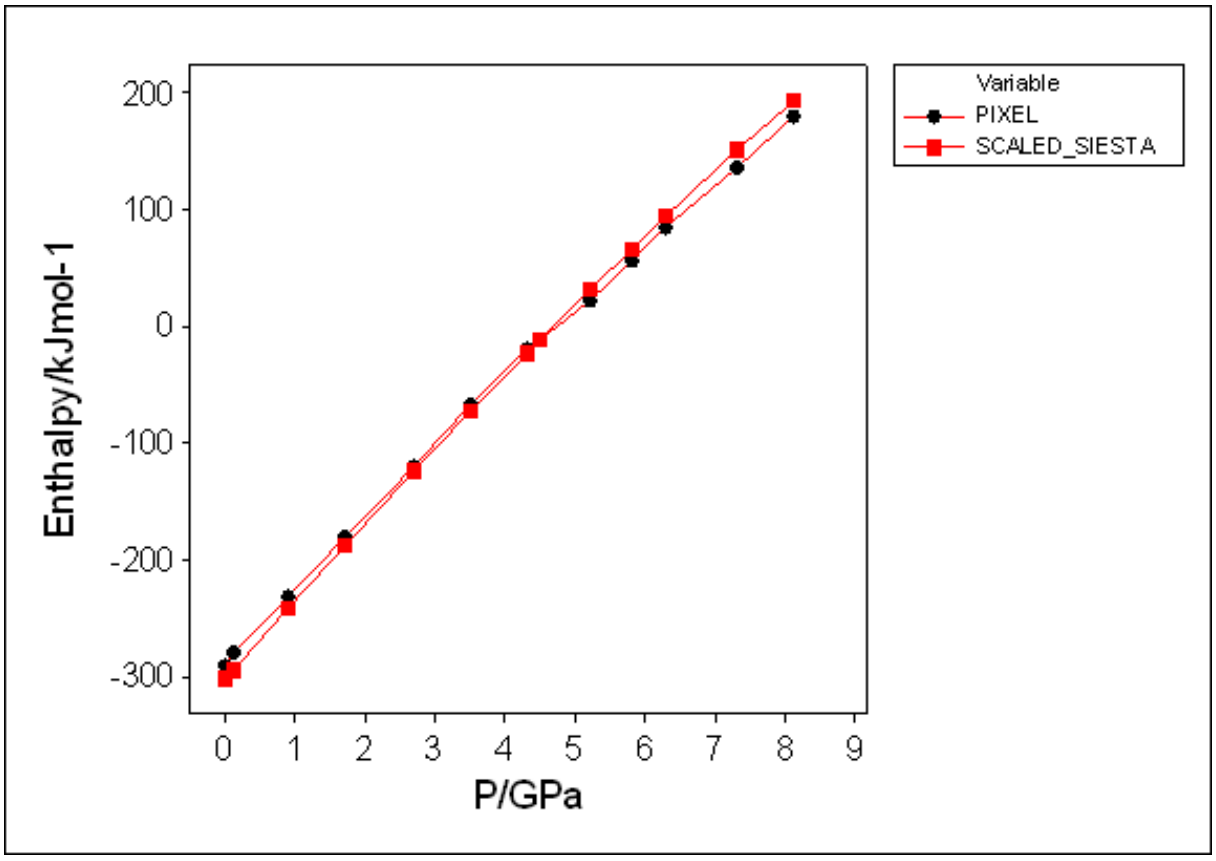

Figure 8: Graph of total interaction energy (as calculated by the *PIXEL* method) for the six most energetically important dimers in the L-serine-I theoretical structure as a function of the distance between the molecular centroids. A line of best fit has been displayed for each interaction. The colour scheme is the same as in Figure 1. Interaction 3 is predominantly a dispersion interaction.

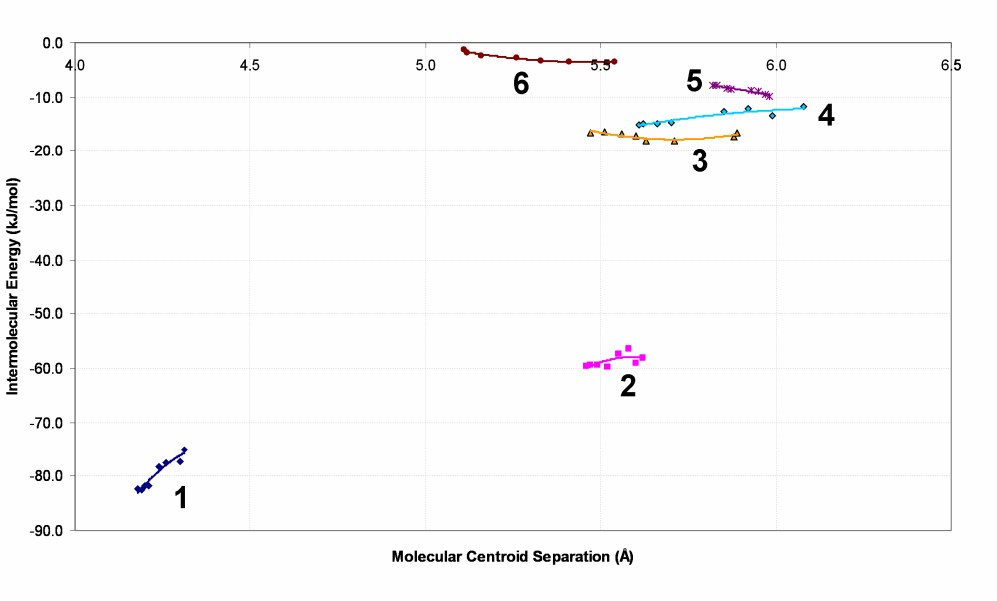

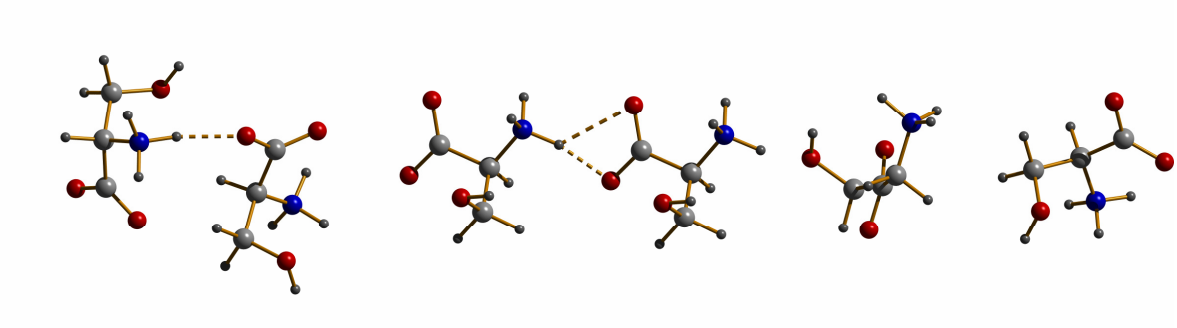

Interaction 1 **Interaction 2** **Interaction 3**

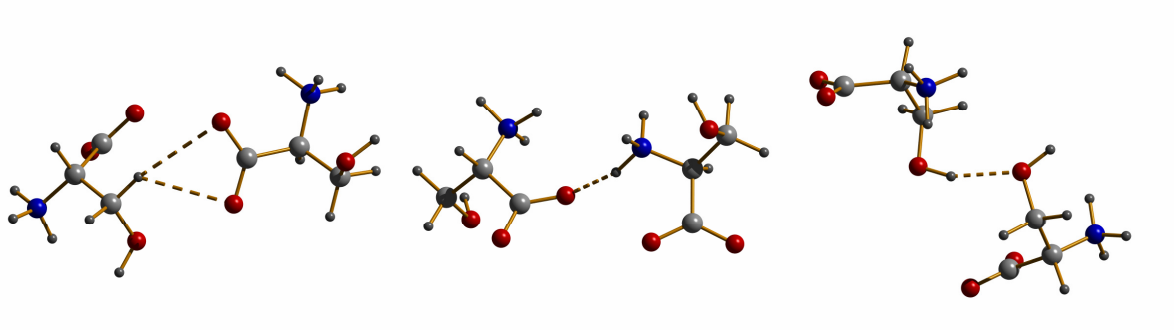

Interaction 4 **Interaction 5** **Interaction 6**

Figure 9: *IsoStar* contoured scatter-plot of an RNH_3^+ contact group around a central $RCOO^-$ group, contoured on the amide-N atoms. The colours show three different levels of contact density with red being the greatest density followed by yellow and then blue. The contact displayed corresponds to the weak NH…O interaction in the structure of L-serine-I (labelled interaction 5 in the *PIXEL* analysis).

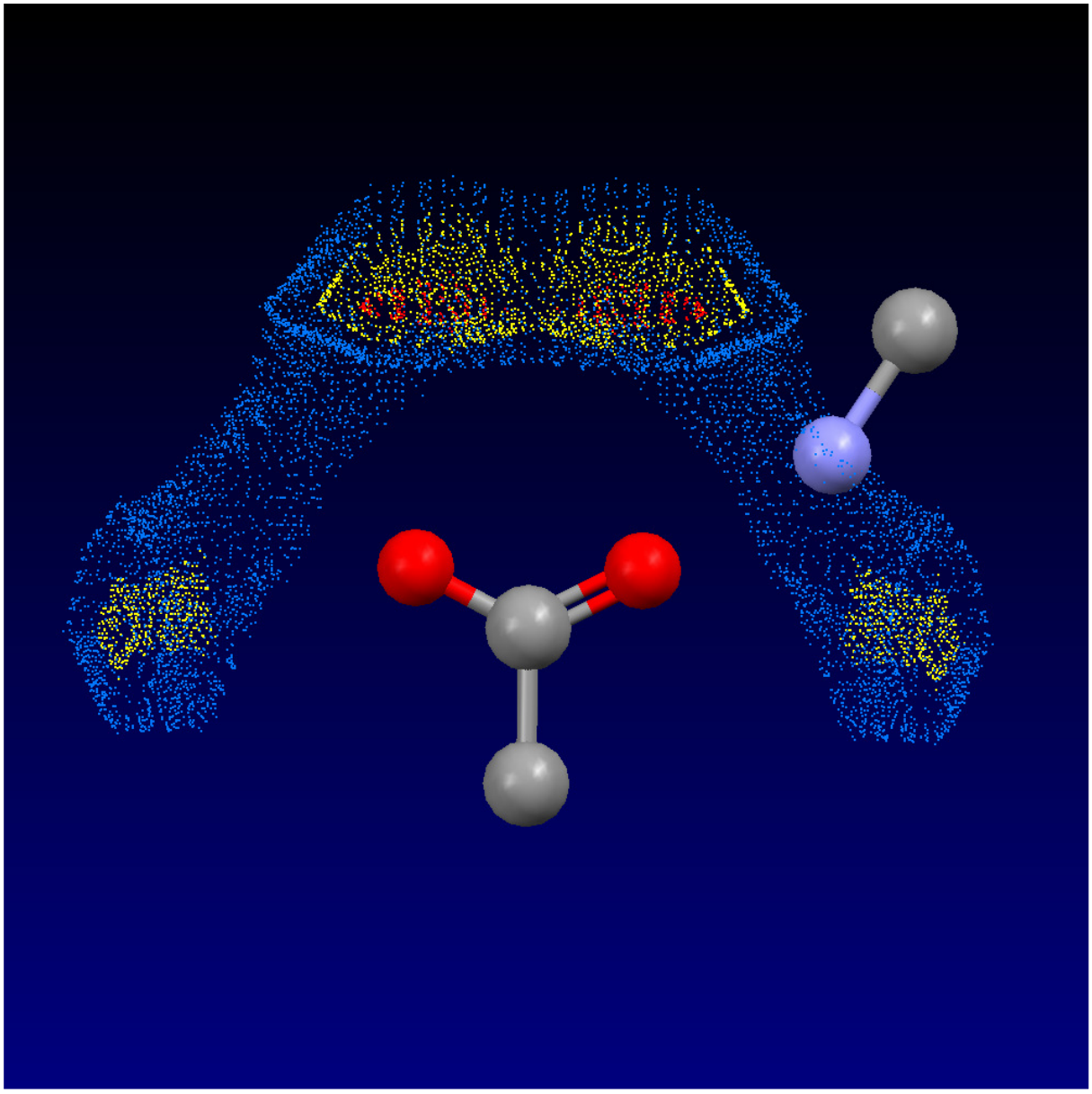

Figure 10: Graph of total interaction energy (as calculated by the *PIXEL* method) for the six most energetically important dimers in the L-serine-II theoretical structure as a function of the distance between the molecular centroids. A line of best fit has been displayed for each interaction. The colour scheme is the same as in Figure 1.

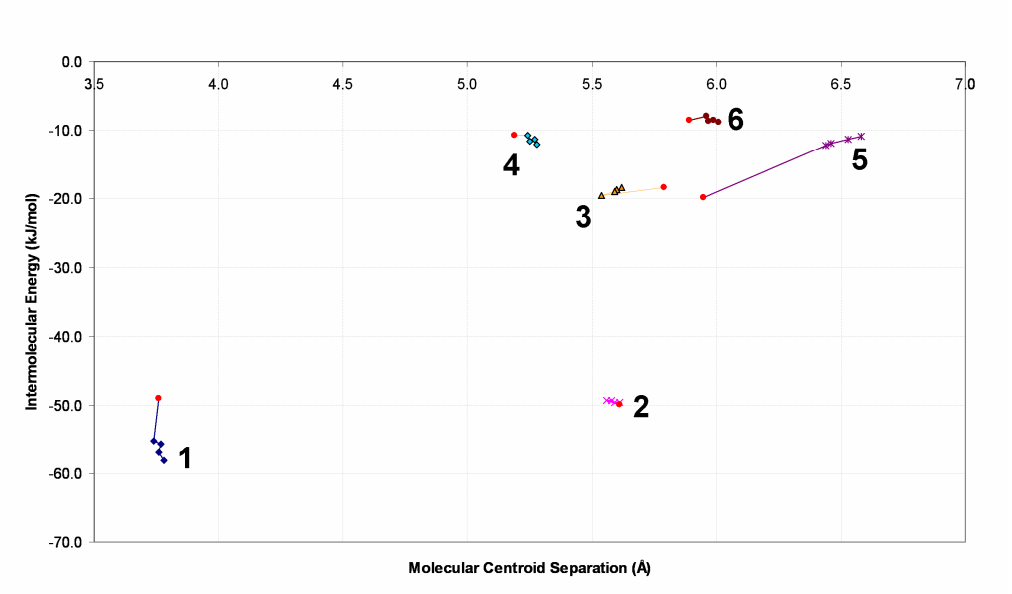

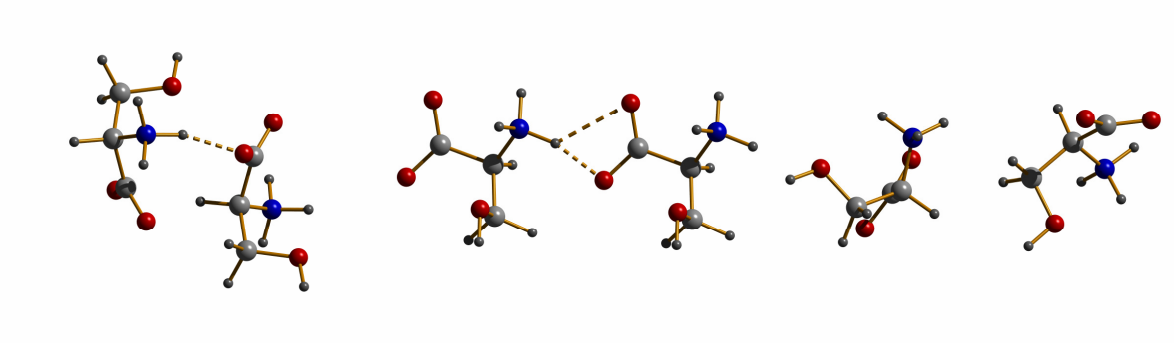

Interaction 1 **Interaction 2** **Interaction 3**

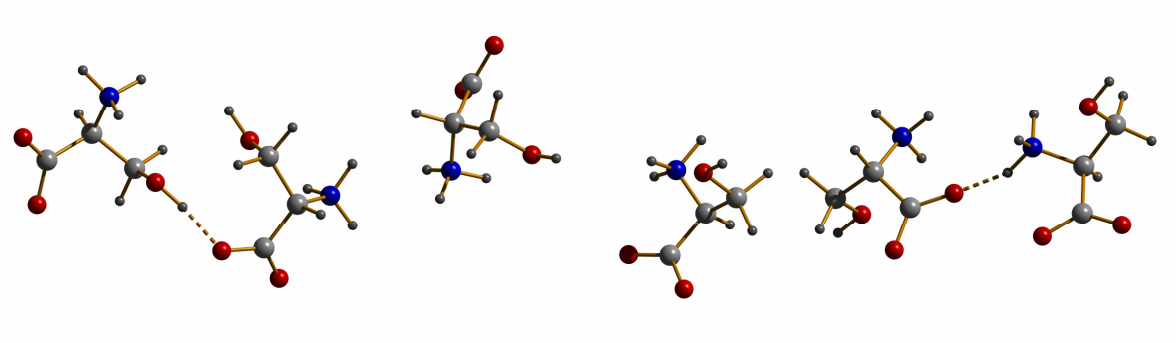

Interaction 4 **Interaction 5** **Interaction 6**